

# A combined density functional and x-ray diffraction study of Pt nanoparticle structure

Matthew Welborn,<sup>1</sup> Wenjie Tang,<sup>1</sup> Jihoon Ryu,<sup>2</sup> Valeri Petkov,<sup>3</sup>  
and Graeme Henkelman<sup>1,a)</sup>

<sup>1</sup>Department of Chemistry and Biochemistry, The University of Texas at Austin, Austin, Texas 78712-0165, USA

<sup>2</sup>Department of Materials Science and Engineering, Korea Advanced Institute of Science and Technology, 291 Daehak-ro, Yuseong-gu, Daejeon 305-701, South Korea

<sup>3</sup>Department of Physics, 203 Dow Science, Central Michigan University, Mt. Pleasant, Michigan 48859, USA

(Received 23 March 2011; accepted 10 June 2011; published online 7 July 2011)

The structure of 1.7 nm Pt nanoparticles is investigated using x-ray diffraction (XRD) measurements and density functional theory (DFT) calculations. Two types of particles are compared, those made by solution chemistry which are capped either by thiol or amine ligands, and dendrimer encapsulated particles (DENs) which do not have capping ligands. All particles were dried before analyzing their structure. Pair distribution function (PDF) data from XRD measurements show that the ligand-capped particles are more disordered than the DENs. To determine the structure of the particles and the nature of the ligand-induced disorder, we use a hybrid reverse Monte Carlo approach. A weighted average of the calculated binding energy of the particles and a goodness-of-fit parameter to the PDF data is taken as the object function, which is minimized to determine the optimal structure. A scan over different weights gives the set of pareto optimal structures, which show how well simultaneous agreement can be reached to both experiment and theory. Using an embedded atom potential to sample configuration space and DFT to refine the optimal structures, we show that the DEN structure is most consistent with a face centered cubic lattice of truncated octahedral shape. The disorder induced by the capping ligands is consistent with surface relaxation of the particle rather than disorder of the crystal structure.

© 2011 American Institute of Physics. [doi:10.1063/1.3607967]

## I. INTRODUCTION

There is considerable interest in properties of particles which arise at the nanoscale. Particularly for surface chemistry, the function of particles is sensitive to the distribution of binding sites, which changes rapidly with size at the nanoscale. To understand the chemical activity of nanoparticle catalysts from a mechanistic point of view, it is essential to determine the surface structure where chemistry takes place.

There are several experimental techniques which can provide structural information of nanoparticles, but no single measurement gives the entire picture. High resolution aberration corrected transmission electron microscopy has atomic resolution, but these measurements must be done in ultra-high vacuum and the high energy electron beam can alter the sample, for example, by heating or electronic reduction. Less invasive techniques based upon x-ray scattering have the advantage of being able to make *in situ* measurements such as in solution within an electrochemical cell.<sup>1</sup>

The extended x-ray adsorption fine structure (EXAFS) provides detailed information about the average distribution of atomic neighbors within a particle. Total x-ray scattering provides complimentary longer range pair distribution function (PDF) data. Both techniques, however, provide only average information about distances between atoms, which does

not uniquely determine the structure of the particles. Suitable models, for example, based upon bulk structures and coordination numbers can be used to infer the structure of nanoscale materials, but there is a possibility of bias when using crystalline materials as a reference for nanoscale structures.<sup>2</sup> Nanoparticles can take icosahedral or irregular structures for which there is no crystalline analog.

The Reverse Monte Carlo (RMC) method is a powerful tool for determining particle structures that are consistent with XRD data.<sup>3</sup> The use of RMC shows, however, that PDF data is generally under-constrained and that there are many structures consistent with the same data.<sup>4</sup> RMC calculations are therefore often combined with constraints, for example, based upon local bonding geometry, to restrict the solution space.<sup>5</sup> A hybrid approach (HRMC), combining RMC with standard Monte Carlo based upon interatomic potentials, is a very attractive way to restrain the optimization of the PDF fit without resorting to *ad hoc* constraints.<sup>6</sup>

In this paper, we use a hybrid approach where the energy of nanoparticle structures are calculated and combined with a goodness-of-fit parameter to the PDF data. A relative weighting factor is used to produce a single object function that is globally minimized to find the optimal particle structure that simultaneously agrees with experiment and theory.

The motivation for this work is the PDF data shown in Fig. 1. Platinum nanoparticles of diameter 1.7 nm with an average of 140 atoms were synthesized using three different techniques: a dendrimer encapsulation method which leaves

<sup>a)</sup> Author to whom correspondence should be addressed. Electronic mail: henkelman@mail.utexas.edu.

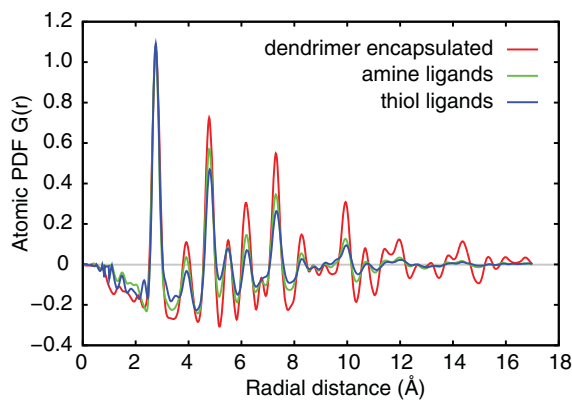


FIG. 1. Pair distribution function data of dry 1.7 nm Pt particles from total x-ray scattering. Dendrimer encapsulated particles have more order than particles capped with ligands, especially at lengths on the order of the diameter of the particle.

the particles largely free of surface ligands and capping methods in which the surface is terminated with either amine or thiol ligands. Details about the synthesis of these particles, as well as the x-ray measurements used to characterize their structure can be found in Ref. 7.

PDF data from total x-ray scattering show a qualitative difference in the structural order on length scales of the particle diameter. The dendrimer encapsulated nanoparticles (DENs) have stronger peaks and more order than the ligand-capped particles. What is not clear from these data is how ordered these particles are in terms of a structural model. The disorder could be due to non-crystallinity throughout the particle or surface relaxations such as those seen in Au nanoparticles<sup>8</sup> and PdSe quantum dots.<sup>9</sup> Ligands have been observed to either increase or decrease the order at particles surfaces,<sup>10</sup> and in some cases have a radical impact on structure as in thiol-capped Au nanoparticles.<sup>11</sup> Here, we propose a framework for combining x-ray scattering data with total energy calculations to help distinguish between these possibilities, and determine the structure of bare and ligand-capped Pt nanoparticles.

## II. METHODS

The goal of the methodology is to combine the strengths of both experiment and theory to give particle structures which are mutually consistent. The PDF data have the clear advantage of being directly taken from the particles that we would like to understand. The data is not sufficient, however, in that many different structures will give rise to the same data in Fig. 1. Calculations of interatomic interactions are valuable in this regard because any particle structure can be evaluated in terms of the binding energy of the particle and hence its stability. The calculations, however, are also not sufficient because numerous experimental details are not included in the atomic models. Solvent, for example, can influence the free energy of the surface and, therefore, the morphology of the particles. The presence of the dendrimer around the DENs is also missing from our calculations, although EXAFS measurements indicate that the interaction between them is weak.<sup>1</sup>

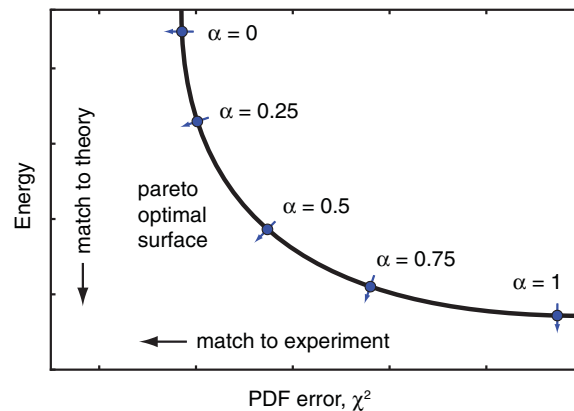


FIG. 2. Illustration of a combined optimization to match both theory (low energy) and experiment (small difference between the pair distribution functions). Optimization with different relative weights for these two objectives,  $\alpha$ , correspond to points on the pareto optimal surface.

Instead of trying to put these details into our calculations, which would greatly increase their complexity, we incorporate them with a combined fit to the experimental data.

A cartoon of the strategy is shown in Fig. 2. We have two objectives, one is to lower the energy and have a stable particle as calculated from theory, and the second is to lower a goodness-of-fit parameter,  $\chi^2$ , to produce a PDF which matches the experimental data. These two objectives are different (even in the sense of their units), but we can define a weight for each which represents the degree to which we trust one over the other, or equivalently, our desire to optimize one over the other.

In Fig. 2, this weight,  $\alpha$ , is the degree to which we try to match the theory, and  $1 - \alpha$  is the degree to which we try to match the experiment;  $\alpha$  defines an optimization direction. A value of  $\alpha = 1$  corresponds to the goal of finding a structure as low in energy as possible without regard to how the corresponding PDF matches the experimental data. The direction of optimization for  $\alpha = 1$  is vertical in Fig. 2. A value of  $\alpha = 0$  corresponds to a horizontal optimization direction in which  $\chi^2$  is minimized so that the calculated PDF matches the experimental as closely as possible without regard to the energy of the structure.

To the extent that there is correlated agreement between experiment and theory, there will be a knee in the pareto optimal curve corresponding to a single optimal solution. The absence of a sharp knee indicates that both objectives cannot be fully optimized and a compromise is necessary. In either case, finding the optimal solution for a given  $\alpha$  is a difficult problem because of the large number of possible nanoparticle structures. A rough objective function surface requires extensive sampling of the landscape and acceleration algorithms to find optimal structures. To help with this sampling, we use an empirical potential as the basis for global optimization, and more accurate quantum calculations for a local refinement of the best candidate structures.

### A. Evaluation of the energy

Two methods were used to evaluate the energy of the particles. An embedded atom method (EAM) potential<sup>12</sup> was

used to describe bare Pt nanoparticles. While this potential does not capture the details of surface relaxation, and cannot be used to model the binding of ligands to the particle surface, it is suitable for sampling large parts of configuration space and identifying structures for refinement by density functional theory (DFT).

The DFT energy of the particles was calculated with the VASP code.<sup>13</sup> The PW91 generalized gradient functional was used to model electron exchange and correlation.<sup>14</sup> Valence electrons were described by a plane wave basis with a cutoff of 230 eV for the Pt nanoparticles, and 400 eV for calculations with ligands. While periodic super-cells were used, the particles (including the ligands) were separated by a vacuum gap of at least 5 Å to avoid inter-particle interactions (bare particles were separated by at least 9 Å). The Brillouin zone was sampled at the  $\Gamma$ -point. States near the Fermi level were averaged using first order Methfessel-Paxton smearing of width 0.2 eV to improve convergence of the total energy. Core electrons were described by pseudopotentials using the projector augmented wave framework.

## B. Evaluation of the PDF error

The pair distribution function of particles was calculated following the method described by Neder and Korsunskiy using<sup>15</sup>

$$G_{\text{calc}}(r) = \frac{A}{r} \sum_{i,j} \frac{1}{2\pi\sigma^2} e^{-\frac{(r-r_{ij})^2}{2\sigma^2}}, \quad (1)$$

where  $r_{ij}$  is the distance between atoms  $i$  and  $j$ ,  $\sigma = 0.02$  Å is the resolution of the experimental data, and  $A$  is a fitting parameter for the amplitude of the signal. Equation (1) differs from that of Neder and Korsunskiy in that a Gaussian function is substituted for their delta function in order to both smooth the PDF and make it differentiable. This change was made so that gradient-based optimizers could be used in the global and local optimization steps. In addition, a baseline term consisting of this function convolved with a Gaussian of width 1 Å was subtracted in order to make the signal vary around zero on this length scale. The goodness-of-fit parameter was calculated as

$$\chi^2 = \frac{1}{R} \int_0^R [G_{\text{expt}}(r) - G_{\text{calc}}(r)]^2 dr, \quad (2)$$

with  $A$  chosen to minimize  $\chi^2$ .

## C. Global optimization

The object function to be minimized,

$$F = \alpha U + (1 - \alpha)\chi^2, \quad (3)$$

is a weighted average of the PDF goodness-of-fit,  $\chi^2$ , and the calculated energy of the particle,  $U$ . Global optimization of  $F$  was performed using a basing hopping algorithm.<sup>16</sup> Trial moves were performed by either displacing a single atom or all atoms. Displacements were chosen from a Gaussian distribution. For the single atom case, the displacement distribution had a standard deviation of 1 Å. For the all atom case, dis-

placement of each atom was chosen from a distribution with a standard deviation of 0.1 Å. Trial moves were accepted based on the Metropolis acceptance probability,

$$P_{\text{acc}} = \min \left[ 1, \exp \left( \frac{-\Delta F}{k_B T} \right) \right], \quad (4)$$

where  $\Delta F$  is the change in the value at the local minimum of the object function in the trial move and  $k_B T$  is the thermal energy in each degree of freedom.

During optimization runs, the temperature was lowered according to a logarithmic schedule from 2000 K to 600 K in 5000 steps. At the highest temperature, the particle was molten and atoms moved around rapidly. The lower temperature was about 100 K below the melting point of the particle, and at this temperature the particle structure changed slowly. At temperatures lower than 600 K, the optimizer was not able to effectively explore the configuration space. A total of 3388 annealing runs were done for each type of particle over a range of  $\alpha$  values from 0.01 to 1.0.

Two technical issues were encountered during the optimization simulations. First, the energy surface had two distinct funnels corresponding to face centered cubic (FCC)-like and icosahedron-like structures with a large barrier and distance between them. Highly disordered structures optimized into the icosahedron-like funnel. In order to explore the space thoroughly, a large number of initial structures were used, including disordered, icosahedron-like, and FCC-like configurations. Second, while  $\chi^2$  is formally smooth and differentiable, it gives rise to small ripples on the surface of the object function,  $F$ . Local minimization of  $F$  was performed by running low temperature (5 K) molecular dynamics to overcome these ripples. At this low temperature, the minimum in an energy basin could be reached without escaping to a different basin.

## III. RESULTS

### A. Dendrimer encapsulated nanoparticles

A global optimization of the structure of the dendrimer encapsulated nanoparticles is shown in Fig. 3. The grey points show the locally optimized energy and  $\chi^2$  values for the large number of local minima sampled. A convex hull shape emerges (black line) containing the pareto optimal surface. The majority of the points on this surface correspond to structures which are FCC-crystallites of truncated octahedral (TO) shape. Each (blue) point along this curve was optimized with a different value of  $\alpha$ .

Two other structures were found to have points near the pareto optimal front, the FCC cuboctahedron (CO) and the icosahedron (IH). Both these structures have magic numbers at the same size as the experimental particles and are often used as models for nanoparticles. The CO structure has essentially the same  $\chi^2$  values as the TO, but is higher in energy as a result of the larger ratio of 100 to 111 face atoms. In experiment, solvent could alter the relative stability of these faces, so we would not want to put too much emphasis on the prediction of TO over CO. While the IH is in fact the most stable particle predicted by the EAM potential, it is unable

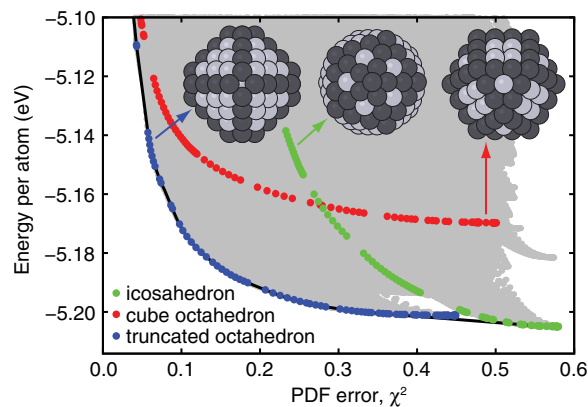


FIG. 3. Global search for nanoparticle structures which both have low energy and match the experimental PDF data for dendrimer encapsulated particles. The range of  $\chi^2$  was chosen to include all values and the range of energy was limited to 0.1 eV per atom above the global minimum, which was considered a limit to the energy required to deform our model structures to those in experiment. Ordered particles with magic numbers of 140 and 147 atoms are shown; edge atoms are highlighted to better show the particle structures.

to reach the low  $\chi^2$  values of the FCC structures. The IH also becomes unfavorable energetically as the structure deforms to match the experimental PDF.

The pareto optimal surfaces for each ordered structure as refined with local DFT optimization are shown in Fig. 4. There are some differences, notably that the IH is energetically unstable with DFT as compared to EAM, but the overall conclusion is the same. The TO structure is the most stable energetically and has the lowest  $\chi^2$ . From this, we conclude that TO shape best describes Pt DENs of this size.

## B. Ligand-capped particles

The same global optimization was done using the experimental PDF data from the amine- and thiol-capped particles. The EAM potential is not able to reproduce the binding of ligands, so we are relying on the experimental data to describe the change in structure due to ligand binding. Figure 5 is similar to Fig. 3 for the DENs. The IH structure gives a somewhat better description of the PDF for particles

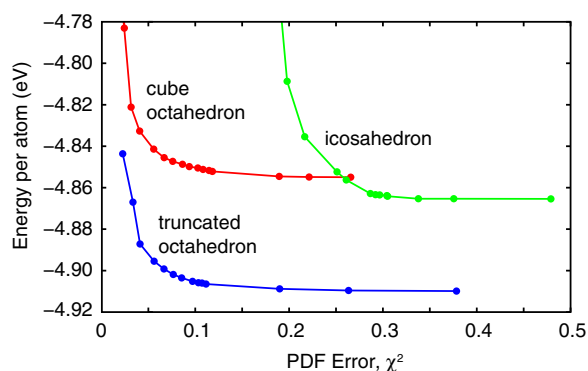


FIG. 4. Local optimization with DFT of the pareto optimal surfaces found by global optimization of the DENs structures.

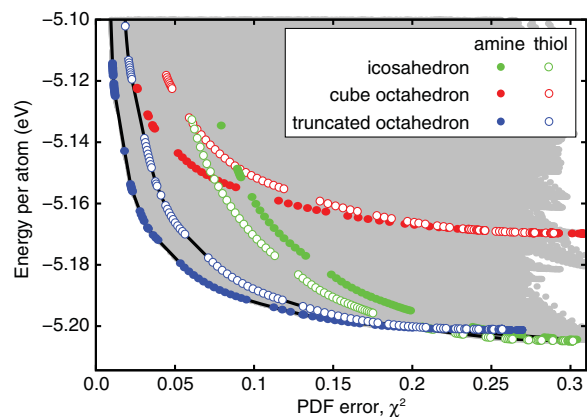


FIG. 5. Global optimization of structures using experimental data for amine- and thiol-capped particles.

with thiol ligands, but as with the DENs, the TO structure is pareto optimal.

A local optimization of the pareto optimal surfaces for the TO structure is shown in Fig. 6. Using DFT, we are able to model the binding of ligands to the particle and test to see if the resulting deformed structures result in a better compromise between experiment and theory. To perform this test, a zero of energy was chosen as that of the DFT optimized structure. A positive energy is then the work required to deform the particle to reduce  $\chi^2$ .

Ligands were bound to the TO particles in the strongest binding edge and corner sites. Figure 7 shows the geometry of the particles with 13 amine and 12 thiol ligands bound to the surface. The surface distortions are relatively small, but they have a significant effect on the PDF. As ligands are added in the model (see Fig. 6), less energy is required to match the experimental PDF. The knee in the pareto optimal curve that develops with ligand binding indicates that these structures are a better common fit to both experiment and theory; in the limit of a sharp knee, there would be a single structure which has both the lowest energy and  $\chi^2$ .

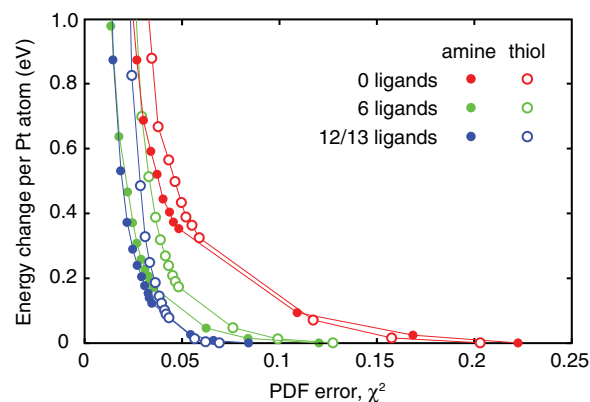


FIG. 6. Local optimization with DFT of the pareto optimal structures found for ligand-bound particles. The addition of ligands in the DFT calculations gives rise to a shape knee in the pareto optimal curves and structures with better agreement between experiment and theory.

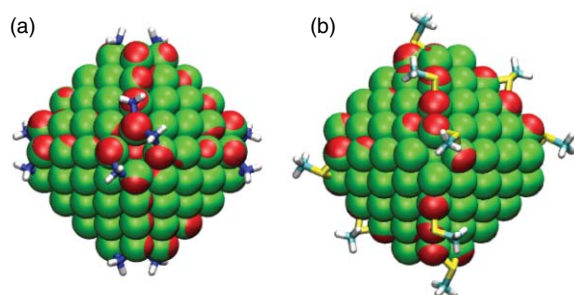


FIG. 7. Surface distortions in nanoparticle structure in ligand-bound nanoparticles (red) as compared to bare (green) particles: (a) 13 amine and (b) 12 thiol ligands.

Figure 8 shows a comparison of the PDF data near the knee in the curves of Figs. 4 and 6, corresponding to a value of  $\alpha = 0.03$ . This point was considered to be near the optimal compromise for achieving both low energy and  $\chi^2$ . It can be seen from this figure that the TO and CO FCC structures give a good description of the experimental PDF structure. The largest error is seen in the DENs data at distances between 12 and 16 Å indicating that even our crystalline particles have too few ordered pairs across their diameter. This could be explained, in part, by solvent ordering at the surface<sup>10</sup> or because the DENs are slightly larger than 140 atoms. With our current model, we were unable to fully reproduce these features without going to unphysical energy scales. The IH, and all other disordered structures in the IH funnel, have clear discrepancies in peaks between 6 and 10 Å. These structures are also found to be unstable energetically from our DFT calculations so that they are not found along the pareto optimal surface.

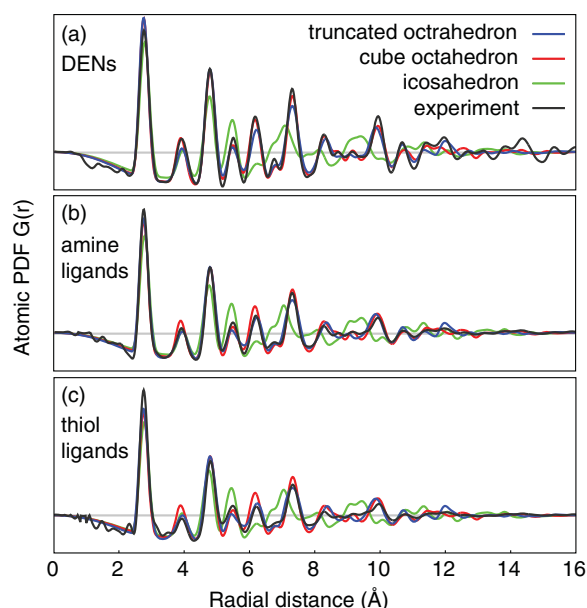


FIG. 8. Comparison of the experimental PDF data with particles from each calculated structure, selected to be near the optimal compromise of low energy and  $\chi^2$ .

## IV. CONCLUSION

With an object function that combines calculated energies and a  $\chi^2$  goodness-of-fit parameter to experimental PDF data, we are able to do a combined optimization of both quantities. Scanning over a weighting parameter between them gives a pareto optimal set of particle structures. A knee in this curve indicates that there are mutually optimal particles which are both energetically stable and fit the experimental PDF data.

In a global optimization of 1.7 nm Pt particles, we find that crystalline FCC particles best match the experimental PDF data from DENs and those with thiol- and amine-capping ligands. The TO is found to be more stable than the CO and therefore offers the best compromise between experiment and theory, although inclusion of solvent in our model could change the surface energy and relative stability of these two FCC structures.

The disorder seen in the experimental PDF from ligand-capped particles as compared to DENs is well described by small surface distortions caused by local relaxation around ligand binding sites. A sharpening of the knee in the pareto optimal curve found using a DFT model with explicit binding of ligands to TO particles edge and corner sites is evidence that this model provides structures which are in better agreement with both theory and experiment.

## ACKNOWLEDGMENTS

The work was funded by the Department of Energy (Contract No. DE-FG02-09ER16090) and the Welch Foundation (Grant No. F-1601). We are grateful to Professor Crooks and his research group for many helpful discussions. Computing time was provided by the Texas Advanced Computing Center and the National Energy Research Scientific Computing Center. Use of the Advanced Photon Source was supported by the U.S. DOE (Contract No. DE-AC02-06CH11357). M.W. was supported as a Beckman Scholar.

- <sup>1</sup>M. R. Knecht, M. G. Weir, V. S. Myers, W. D. Pyrz, H. Ye, V. Petkov, D. J. Buttrey, A. I. Frenkel, and R. M. Crooks, *Chem. Mater.* **20**, 5218 (2008).
- <sup>2</sup>V. Petkov, N. Bedord, M. R. Knecht, M. G. Weir, R. M. Crooks, W. Tang, G. Henkelman, and A. Frenkel, *J. Phys. Chem. C* **112**, 8907 (2008).
- <sup>3</sup>R. L. McGreevy and L. Pusztai, *Mol. Simul.* **1**, 359 (1988).
- <sup>4</sup>R. L. McGreevy, *J. Phys.: Condens. Matter* **13**, R877 (2001).
- <sup>5</sup>G. Evrard and L. Pusztai, *J. Phys.: Condens. Matter* **17**, S1 (2005).
- <sup>6</sup>G. Opletal, T. Petersen, B. O(tm)Malley, I. Snook, D. G. McCulloch, N. A. Marks, and I. Yarovsky, *Mol. Simul.* **28**, 927 (2002).
- <sup>7</sup>C. Dablemont, P. Lang, C. Mangeney, J.-Y. Piquemal, V. Petkov, F. Herbst, and G. Viau, *Langmuir* **24**, 5832 (2008).
- <sup>8</sup>W. J. Huang, R. Sun, J. Tao, L. D. Menard, R. G. Nuzzo, and J. M. Zuo, *Nature Mater.* **7**, 308 (2008).
- <sup>9</sup>V. Petkov, I. Moreels, Z. Hens, and Y. Ren, *Phys. Rev. B* **81**, 241304 (2010).
- <sup>10</sup>H. Zhang, B. Chen, Y. Ren, G. A. Waychunas, and J. F. Banfield, *Phys. Rev. B* **81**, 125444 (2010).
- <sup>11</sup>P. D. Jadzinsky, G. Calero, C. J. Ackerson, D. A. Bushnell, and R. D. Kornberg, *Science* **318**, 430 (2007).
- <sup>12</sup>C. L. Liu, J. M. Cohen, J. B. Adams, and A. F. Voter, *Surf. Sci.* **253**, 334 (1991).
- <sup>13</sup>G. Kresse and D. Joubert, *Phys. Rev. B* **59**, 1758 (1999).
- <sup>14</sup>J. P. Perdew, in *Electronic Structure of Solids*, edited by P. Ziesche and H. Eschrig (Akademie Verlag, Berlin, 1991), pp. 11–20.
- <sup>15</sup>R. B. Neder and V. I. Korsunskiy, *J. Phys.: Condens. Matter* **17**, S125 (2005).
- <sup>16</sup>D. J. Wales and J. P.K. Doye, *J. Phys. Chem. A* **101**, 5111 (1999).